Three-layer dielectric models for generalized Coulomb potential calculation in ellipsoidal geometry

Changfeng Xue and Shaozhong Deng

Phys. Rev. E **83**, 056709 — Published 19 May 2011

DOI: 10.1103/PhysRevE.83.056709

Three-layer dielectric models for generalized Coulomb potential calculation in ellipsoidal geometry

Changfeng Xue[1] and Shaozhong Deng[2,*]

[1]*Department of Fundamental Sciences,*

Yancheng Institute of Technology, Yancheng, Jiangsu 224051, PR China

[2]*Department of Mathematics and Statistics,*

University of North Carolina at Charlotte, Charlotte, NC 28223-0001, USA

Abstract

This paper concerns a basic electrostatic problem: How to calculate generalized Coulomb and self-polarization potentials in heterogeneous dielectric media. In particular, with simulations of ellipsoidal semi-conductor quantum dots and elongated bio-macromolecules being its target applications, this paper extends the so-called three-layer dielectric models for generalized Coulomb and self-polarization potential calculation from the spherical and the spheroidal geometries to the tri-axial ellipsoidal geometry. Compared to the simple step-like dielectric model, these three-layer dielectric models can overcome the mathematical divergence in the self-polarization energy by employing continuous radial dielectric functions. More specifically, in this paper, the novel quasi-harmonic three-layer dielectric model for the ellipsoidal geometry is first discussed, and the explicit analytical series solutions of the corresponding electrostatic problem are obtained in terms of the ellipsoidal harmonics. Then, a robust numerical procedure working for general three-layer dielectric models is developed. The key component of the numerical method is to subdivide the transition layer of the underlying three-layer model into multiple sublayers, and then in each one of them approximate the select dielectric function of the transition layer by one of the quasi-harmonic functional form rather than simply by a constant value as one would normally do. As the result, the numerical method has no numerical divergence.

PACS numbers: 02.70.-c; 82.20.Wt; 41.20.Cv; 73.21.La

Keywords: Generalized Coulomb potential; Self-polarization energy; Poisson equation; Dielectric mismatch

*Corresponding author: shaodeng@uncc.edu

I. INTRODUCTION

As in [1], in this paper we are concerned with the calculation of the generalized Coulomb potential energy V_c and the self-polarization potential energy V_s involving a dielectric object. The generalized Coulomb potential energy V_c between two particles inside or outside a dielectric object with the coordinates $\mathbf{r}$ and $\mathbf{r}_s$, and the charges e and e_s, respectively, can be evaluated through $V_c(\mathbf{r}, \mathbf{r}_s) = e\Phi(\mathbf{r}, \mathbf{r}_s)$, where $\Phi(\mathbf{r}, \mathbf{r}_s)$ is the electrostatic potential that verifies the Poisson equation

$$\nabla \cdot \varepsilon(\mathbf{r}) \nabla \Phi(\mathbf{r}, \mathbf{r}_s) = -4\pi e_s \delta(\mathbf{r} - \mathbf{r}_s). \tag{1}$$

On the other hand, the self-polarization potential energy V_s of the particle e can be calculated from $V_c(\mathbf{r}, \mathbf{r}_s)$ by taking $\mathbf{r} = \mathbf{r}_s$ and $e = e_s$, excluding the direct Coulomb interaction from $\Phi(\mathbf{r}, \mathbf{r}_s)$, and dividing by 2 as it corresponds to a self-energy, namely, $V_s(\mathbf{r}) = \frac{1}{2} e\Phi(\mathbf{r}, \mathbf{r})$. In (1), $\varepsilon(\mathbf{r})$ is the dielectric function which in general could be spatially dependent, and $\delta(\ldots)$ is the Dirac delta function, respectively. Two representative areas of application of such an electrostatic problem include the simulation of semi-conductor quantum dots (QDs) with finite confinement barriers [2–4], and the calculation of electrostatic interactions in the so-called hybrid explicit/implicit solvation models for bio-molecular simulations [5].

For simplicity, in most theoretical studies of the underlying applications, macroscopic dielectric constants ε_i and ε_o are assigned for the object (a QD or the dielectric cavity in a hybrid solvation model) and the surrounding medium (the QD matrix or the implicit solvent in the hybrid solvation model), respectively. In this case, explicit analytical series solutions of the generalized Coulomb and the self-polarization potential energies exist for both the spherical and the spheroidal geometries [6–9], but unfortunately, in addition to the unphysicality of the sharp jump in the dielectric constant at the object surface, there is also a major disadvantage of this step-like model. In particular, all induced polarization charges will be localized at the object surface of zero width so both the real and the induced charges can coincide at the same location, giving rise to a self-polarization energy that diverges at the object surface.

To remove such mathematical divergence of the step-like dielectric model, the so-called three-layer dielectric models have been proposed in which the step-like dielectric function is replaced by a radially dependent continuous dielectric function $\varepsilon(\mathbf{r})$ that changes smoothly from the object value ε_i to the medium value ε_o within a thin transition layer around the

object surface. As a consequence of using such a three-layer dielectric model, the induced charges are spread along the transition layer and the mathematical divergence in the self-polarization energy disappears. Moreover, in the case of the spherical geometry, a novel three-layer dielectric model, called the quasi-harmonic model, has been proposed, the corresponding electrostatic problem still admitting explicit analytical series solutions [10, 11], while for general three-layer dielectric models several procedures have been developed for solving the problem numerically [4, 11–13]. Later, the quasi-harmonic three-layer dielectric model and the robust numerical procedure particularly developed in [11] were extended to the spheroidal geometry [1, 14].

In this paper, we shall further extend the quasi-harmonic three-layer dielectric model and the robust numerical method for general three-layer dielectric models from the spheroidal coordinates to one of the most general three-dimensional coordinates in which the Laplace equation is separable [15], the tri-axial ellipsoidal coordinates [16–20]. This extension may be needed since, for example, realistic quantum dots might be neither perfect spheres nor perfect spheroids, while it has been shown that a small change in the external shape of a QD may strongly influence the energy spectrum and other characteristics of such a semi-conductor structure [21–24]. On the other hand, in the hybrid solvation models for bio-molecular simulations, for non-spherical or non-spheroidal bio-macromolecules, from computational point of view, it may be more beneficial to adopt ellipsoidal cavities that can conform closely to the irregular shapes of the bio-molecules. What makes the proposed extension even more important is the fact that, among the eleven coordinate systems in which the Laplace equation (more precisely, the Helmholtz equation) is separable, the other ten coordinate systems can be considered as degenerate forms of the ellipsoidal one [15].

The paper is organized as follows. In Section II, we briefly review the ellipsoidal coordinates and the ellipsoidal harmonics. In Section III, we present the analytical solution of the electrostatic problem with using the step-like dielectric model. Then the analytical solution corresponding to the quasi-harmonic three-layer dielectric model is given in Section IV, and a robust numerical method working for general three-layer dielectric models is described in Section V. Finally, results of some illustrative numerical experiments are presented in Section VI, and a few concluding remarks are given in Section VII.

II. LAPLACE EQUATION IN ELLIPSOIDAL COORDINATES

In order to solve the Laplace equation in a domain bounded (internally or externally) by a tri-axial ellipsoidal surface, it is convenient to formulate the problem in ellipsoidal coordinates. Several definitions of these coordinates exist, and we adopt here Hobson's formalism [25] which appears to have become dominant in problems involving ellipsoidal boundaries [16–19, 26, 27]. The ellipsoidal coordinates (ξ, μ, ν) corresponding to the point (x, y, z) in the rectangular coordinates, generated by a reference ellipsoid

$$\frac{x^2}{a^2} + \frac{y^2}{b^2} + \frac{z^2}{c^2} = 1, \tag{2}$$

where $a > b > c > 0$ are its semi-axes, satisfy

$$\frac{x^2}{\lambda^2} + \frac{y^2}{\lambda^2 - h^2} + \frac{z^2}{\lambda^2 - k^2} = 1, \tag{3}$$

where λ stands for either ξ, μ, or ν. The two constants k and h are determined by the semi-focal distances of the reference ellipsoid, namely, $k = \sqrt{a^2 - c^2}$ and $h = \sqrt{a^2 - b^2}$. Note that every ellipsoidal coordinate has the physical dimension of distance, each one being defined in the intervals $0 \leq \nu^2 \leq h^2 \leq \mu^2 \leq k^2 \leq \xi^2 < \infty$. The surface of ξ = constant is a tri-axial ellipsoid of semi-axes ξ, $\sqrt{\xi^2 - h^2}$ and $\sqrt{\xi^2 - k^2}$; in particular, $\xi = a$ corresponds to the reference ellipsoid (2). Recall that for spherical coordinates, a constant radius r defines a single sphere. Therefore, analogously the variable ξ in the ellipsoidal coordinate system is called radial and assumes only positive values, namely, $\xi \in [k, \infty)$. The surface of μ = constant is a hyperboloid of one sheet and that of ν = constant a hyperboloid of two sheets. Unlike the radial coordinate ξ, both angular coordinates μ and ν may also be negative.

The transformation between the ellipsoidal and the Cartesian coordinates is [25]

$$x^2 = \frac{\xi^2 \mu^2 \nu^2}{k^2 h^2}, \tag{4a}$$

$$y^2 = \frac{(\xi^2 - h^2)(\mu^2 - h^2)(h^2 - \nu^2)}{h^2 (k^2 - h^2)}, \tag{4b}$$

$$z^2 = \frac{(\xi^2 - k^2)(k^2 - \mu^2)(k^2 - \nu^2)}{k^2 (k^2 - h^2)}. \tag{4c}$$

The Laplace equation is separable in the ellipsoidal coordinates. As a matter of fact, each

of the three ellipsoidal variables satisfies the same Lamé differential equation

$$\left(\lambda^2-h^2\right)\ \left(\lambda^2-k^2\right)\frac{\mathrm{d}^2E(\lambda)}{\mathrm{d}\lambda^2}+\lambda\left(2\lambda^2-h^2-k^2\right)\frac{\mathrm{d}E(\lambda)}{\mathrm{d}\lambda}$$
$$+\left[\left(h^2+k^2\right)q-n(n+1)\lambda^2\right]E(\lambda)=0, \tag{5}$$

where q is an arbitrary constant to be fixed appropriately [15].

The solutions of (5), E_n^p, are called Lamé functions of the first kind of degree n and order p. Here both indices n and p are positive integers satisfying $2n+1\geq p\geq 1$. For the determination of the Lamé functions, see e.g., [15], for a short list of the Lamé functions of the first kind, see e.g., [19], and for numerical computation of the Lamé functions, see e.g., [26, 28, 29]. In particular, Ref. [26] has all necessary details about computation of Lamé functions including discussions on potential problems for accurate calculation and possible solutions, which greatly helped the authors carry out this study successfully.

A general internal ellipsoidal harmonic which is a normal solution of the Laplace equation and is regular at the origin may be written in terms of the Lamé product as

$$\mathcal{E}_n^p(\mathbf{r})=E_n^p(\xi)E_n^p(\mu)E_n^p(\nu). \tag{6}$$

Similarly, an external ellipsoidal harmonic which is regular at infinity is defined as

$$\mathcal{F}_n^p(\mathbf{r})=F_n^p(\xi)E_n^p(\mu)E_n^p(\nu), \tag{7}$$

where $F_n^p(\xi)$ is the Lamé function of the second kind of degree n and order p, which is related to the corresponding Lamé function of the first kind $E_n^p(\xi)$ by [25]

$$F_n^p(\xi)=(2n+1)E_n^p(\xi)\int_\xi^\infty\frac{\mathrm{d}\xi'}{[E_n^p(\xi')]^2\sqrt{\left(\xi'^2-h^2\right)\left(\xi'^2-k^2\right)}}. \tag{8}$$

Both the internal $\mathcal{E}_n^p(\mathbf{r})$ and the external $\mathcal{F}_n^p(\mathbf{r})$ ellipsoidal harmonics are linearly independent and form a complete set of functions. Moreover, there exists an orthogonality relation of the Lamé functions of the first kind as [19, 26]

$$\int_0^h\int_h^k\frac{E_n^p(\mu)E_n^p(\nu)E_{n'}^{p'}(\mu)E_{n'}^{p'}(\nu)\left(\mu^2-\nu^2\right)}{\sqrt{\left(\mu^2-h^2\right)\left(k^2-\mu^2\right)\left(h^2-\nu^2\right)\left(k^2-\nu^2\right)}}\mathrm{d}\mu\mathrm{d}\nu=\gamma_n^p\delta_{nn'}\delta_{pp'}, \tag{9}$$

where the Kronecker delta $\delta_{ij}=1$ when $i=j$ and is zero otherwise, and the normalization constant γ_n^p is

$$\gamma_n^p=\int_0^h\int_h^k\frac{\left[E_n^p(\mu)E_n^p(\nu)\right]^2\left(\mu^2-\nu^2\right)}{\sqrt{\left(\mu^2-h^2\right)\left(k^2-\mu^2\right)\left(h^2-\nu^2\right)\left(k^2-\nu^2\right)}}\mathrm{d}\mu\mathrm{d}\nu. \tag{10}$$

A list of normalization constants γ_n^p of low orders can be found in [19]. In particular, $\gamma_0^1 = \pi/2$ under the definition of (10).

Furthermore, as is well known, it is often essential in solving harmonic boundary-value problems to have an expansion for the reciprocal distance (the basic potential given by the Green's function). Using the orthogonality relation (9), the expansion for the reciprocal distance in the ellipsoidal coordinates can also be constructed [19], namely,

$$\frac{1}{|\mathbf{r}-\mathbf{r}_s|} = \begin{cases} \displaystyle\sum_{n=0}^{\infty}\sum_{p=1}^{2n+1} \mathcal{K}_{np}\mathcal{E}_n^p(\mathbf{r}_s)\mathcal{F}_n^p(\mathbf{r}), & \text{if } \xi \geq \xi_s, \\ \displaystyle\sum_{n=0}^{\infty}\sum_{p=1}^{2n+1} \mathcal{K}_{np}\mathcal{F}_n^p(\mathbf{r}_s)\mathcal{E}_n^p(\mathbf{r}), & \text{if } \xi \leq \xi_s, \end{cases} \tag{11}$$

where the coefficient $\mathcal{K}_{np}$ is

$$\mathcal{K}_{np} = \frac{\pi}{2(2n+1)\gamma_n^p}. \tag{12}$$

It is noteworthy that the orthogonality relation, the normalization constants, and accordingly the expansion of the reciprocal distance all are given in a slightly different way in [16, 18, 30], where the double integral involved is carried over the whole surface of the ellipsoid $\xi = a$ (rather than $\int_0^h \int_h^k$). As the consequence, the corresponding normalization constant are eight times of those given by (10) [31], with $\gamma_0^1 = 4\pi$. Therefore, if the normalization constants presented in [16, 18, 30] are used, then

$$\mathcal{K}_{np} = \frac{4\pi}{(2n+1)\gamma_n^p}. \tag{13}$$

The Lam*é* functions $E_n^p(\xi)$ and the products $E_n^p(\mu)E_n^p(\nu)$ are analogous to the radial functions $R_l^m(r)$ and the surface spherical harmonics $Y_l^m(\theta,\phi)$ in the spherical harmonic theory. For this reason, products of the form $E_n^p(\mu)E_n^p(\nu)$ are called surface ellipsoidal harmonics through this paper. It may also be noted that when $\xi \to \infty$, $E_n^p(\xi) \sim c_0\xi^n$ and $F_n^p(\xi) \sim E_n^p(\xi)/\xi^{2n+1} \sim c_0/\xi^{n+1}$ which corresponds to the $r^{-(n+1)}$-potential term in the spherical system [19].

To conclude this section, we introduce some shorthand notations in order to make later formulations easier. We denote the summation $\sum_{n=0}^{\infty}\sum_{p=1}^{2n+1}$ simply by $\hat{\sum}$. Also, for $n = 0, 1, \cdots$, and $p = 1, 2, \cdots, 2n+1$, we let $u_{np}(\xi)$ and $v_{np}(\xi)$ be the ratios of the Lam*é* functions of the first and the second kinds, namely,

$$u_{np}(\xi) = \frac{E_n^p(\xi)}{F_n^p(\xi)} \qquad \text{and} \qquad v_{np}(\xi) = \frac{F_n^p(\xi)}{E_n^p(\xi)}, \tag{14}$$

and $\widetilde{E_n^p}(\xi)$ and $\widetilde{F_n^p}(\xi)$ be the logarithmic derivatives of the Lamé functions, namely,

$$\widetilde{E_n^p}(\xi) = \frac{E_n^{p\prime}(\xi)}{E_n^p(\xi)} \qquad \text{and} \qquad \widetilde{F_n^p}(\xi) = \frac{F_n^{p\prime}(\xi)}{F_n^p(\xi)}. \tag{15}$$

III. ANALYTICAL SOLUTION FOR THE STEP-LIKE DIELECTRIC MODEL

The three-dimensional solution of the Poisson equation (1) is quite complicated to find even by assuming the ellipsoidal geometry and only the radial ξ-dependence of $\varepsilon(\mathbf{r})$. Nevertheless, it can be solved analytically if the radial dependence of $\varepsilon(\mathbf{r})$ corresponds to the simple step-like model, as shown in Fig. 1, in which two constant dielectric permittivities ε_i and ε_o are assigned for the ellipsoidal object and the surrounding medium, respectively. Let the dielectric ellipsoid be centered at the origin and defined by (2). In terms of the ellipsoidal coordinates (ξ, μ, ν) defined in Section II, the surface of the ellipsoid is given by $\xi = \xi_b = a$. Then the step-like dielectric model is defined by

$$\varepsilon(\xi) = \begin{cases} \varepsilon_i, & \text{if } \xi \leq \xi_b, \\ \varepsilon_o, & \text{if } \xi > \xi_b. \end{cases} \tag{16}$$

The explicit analytical solution of the corresponding electrostatic problem (1) has not been published in the literature, to the best of the authors' knowledge, and thus shall be discussed first for the completeness of the paper.

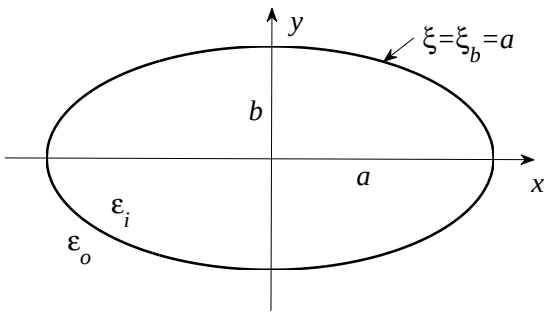

FIG. 1: Schematic illustration of the step-like dielectric model: the dielectric constants of an ellipsoid and the surrounding medium are ε_i and ε_o, respectively. The surface of the ellipsoid is $\xi = \xi_b = a$. The graph shown represents the xy-cross section of the ellipsoid.

Let us begin by considering the case that the point charge e_s is located at the point $\mathbf{r}_\mathrm{s} = (\xi_s, \mu_s, \nu_s)$ inside the ellipsoid. In this case, the electrostatic potential must be finite

at infinity so the potential Φ_o outside the ellipsoid ($\xi_b \le \xi$) shall be expanded in terms of the external harmonics $\mathcal{F}_n^p(\mathbf{r})$. On the other hand, the potential Φ_i inside the ellipsoid ($k \le \xi \le \xi_b$) due to the point charge e_s alone is $e_s/\varepsilon_i|\mathbf{r}-\mathbf{r}_s|$. We must superimpose on this direct Coulomb potential a finite reaction potential due to the polarization of the dielectric, which shall be expanded in terms of the internal harmonics $\mathcal{E}_n^p(\mathbf{r})$. In short, the electrostatic potential Φ_o or Φ_i at a field point $\mathbf{r} = (\xi, \mu, \nu)$ outside or inside the ellipsoid, respectively, due to a point charge e_s at the point $\mathbf{r}_s$ inside the ellipsoid (so $\xi_b > \xi_s \ge k$) takes the form

$$\Phi_o(\mathbf{r}, \mathbf{r}_s) = \frac{e_s}{\sqrt{\varepsilon_i \varepsilon_o}} \hat{\sum} A_{np}^{(1)} \cdot \mathcal{K}_{np} \mathcal{E}_n^p(\mathbf{r}_s) \mathcal{F}_n^p(\mathbf{r}), \tag{17a}$$

$$\Phi_i(\mathbf{r}, \mathbf{r}_s) = \frac{e_s}{\varepsilon_i|\mathbf{r}-\mathbf{r}_s|} + \frac{e_s}{\varepsilon_i} \hat{\sum} B_{np}^{(1)} \cdot v_{np}(\xi_b) \mathcal{K}_{np} \mathcal{E}_n^p(\mathbf{r}_s) \mathcal{E}_n^p(\mathbf{r}). \tag{17b}$$

Note that here factors such as $\mathcal{K}_{np}\mathcal{E}_n^p(\mathbf{r}_s)$, e_s/ε_i and $e_s/\sqrt{\varepsilon_i\varepsilon_o}$ are extracted from expansion coefficients of the ellipsoidal harmonics explicitly so that, $A_{np}^{(1)}$ and $B_{np}^{(1)}$, the remaining parts of the expansion coefficients, depend neither on the source charge nor on the particular dielectric values of ε_i and ε_o. Rather, as to be shown below, they depend only on the ellipsoidal surface $\xi = \xi_b$ and the dielectric mismatch ratio $\varepsilon_r = \varepsilon_i/\varepsilon_o$, and thus only need to be calculated once even if there are many source charges present and the positions of these charges change over time, a typical situation in hybrid-solvation bio-molecular simulations.

The unknown constant expansion coefficients $A_{np}^{(1)}$ and $B_{np}^{(1)}$ in (17) can be determined by the boundary condition on the ellipsoidal surface $\xi = \xi_b$ which, under the ellipsoidal coordinates, is

$$\Phi_o|_{\xi=\xi_b} = \Phi_i|_{\xi=\xi_b} \quad \text{and} \quad \varepsilon_o \frac{\partial \Phi_o}{\partial \xi}\bigg|_{\xi=\xi_b} = \varepsilon_i \frac{\partial \Phi_i}{\partial \xi}\bigg|_{\xi=\xi_b}, \tag{18}$$

the orthogonality relation of the surface ellipsoidal harmonics (9), and the known expansion of the reciprocal distance in the ellipsoidal coordinates (11). Omitting all details, for $n = 0, 1, \cdots$, and $p = 1, 2, \cdots, 2n+1$, we can obtain

$$\begin{bmatrix} \sqrt{\varepsilon_r}, & -1 \\ \widetilde{F_n^p}(\xi_b), & -\sqrt{\varepsilon_r}\widetilde{E_n^p}(\xi_b) \end{bmatrix} \begin{pmatrix} A_{np}^{(1)} \\ B_{np}^{(1)} \end{pmatrix} = \begin{pmatrix} 1 \\ \sqrt{\varepsilon_r}\widetilde{F_n^p}(\xi_b) \end{pmatrix}. \tag{19}$$

Similarly, if the source charge e_s is located at the point $\mathbf{r}_s = (\xi_s, \mu_s, \nu_s)$ outside the ellipsoid (so $\xi_s \ge \xi_b > k$), the electrostatic potential Φ_o or Φ_i takes the form

$$\Phi_o(\mathbf{r}, \mathbf{r}_s) = \frac{e_s}{\varepsilon_o|\mathbf{r}-\mathbf{r}_s|} + \frac{e_s}{\varepsilon_o} \hat{\sum} A_{np}^{(2)} \cdot u_{np}(\xi_b) \mathcal{K}_{np} \mathcal{F}_n^p(\mathbf{r}_s) \mathcal{F}_n^p(\mathbf{r}), \tag{20a}$$

$$\Phi_i(\mathbf{r}, \mathbf{r}_s) = \frac{e_s}{\sqrt{\varepsilon_i \varepsilon_o}} \hat{\sum} B_{np}^{(2)} \cdot \mathcal{K}_{np} \mathcal{F}_n^p(\mathbf{r}_s) \mathcal{E}_n^p(\mathbf{r}), \tag{20b}$$

where the expansion coefficients $A_{np}^{(2)}$ and $B_{np}^{(2)}$ are given by

$$\left[\begin{array}{cc} \sqrt{\varepsilon_r}, & -1 \\ \widetilde{F_n^p}(\xi_b), & -\sqrt{\varepsilon_r}\widetilde{E_n^p}(\xi_b) \end{array} \right] \left(\begin{array}{c} A_{np}^{(2)} \\ B_{np}^{(2)} \end{array} \right) = \left(\begin{array}{c} -\sqrt{\varepsilon_r} \\ -\widetilde{E_n^p}(\xi_b) \end{array} \right). \tag{21}$$

Recall that the self-polarization potential energy $V_s(\mathbf{r})$ of the particle e is calculated from the generalized Coulomb potential energy $V_c(\mathbf{r}, \mathbf{r}_s) = e\Phi(\mathbf{r}, \mathbf{r}_s)$ by taking $\mathbf{r} = \mathbf{r}_s$ and $e = e_s$, excluding the direct Coulomb interaction from $\Phi(\mathbf{r}, \mathbf{r}_s)$, and then dividing by 2, namely, $V_s(\mathbf{r}) = \frac{1}{2}e\Phi(\mathbf{r}, \mathbf{r})$. From (17b) and (20a), we obtain

$$V_s(\mathbf{r}) = \begin{cases} \dfrac{e^2}{2\varepsilon_o}\hat{\sum} A_{np}^{(2)} \cdot u_{np}(\xi_b)\mathcal{K}_{np}\mathcal{F}_n^{p2}(\mathbf{r}), & \text{if } \xi \geq \xi_b, \\ \dfrac{e^2}{2\varepsilon_i}\hat{\sum} B_{np}^{(1)} \cdot v_{np}(\xi_b)\mathcal{K}_{np}\mathcal{E}_n^{p2}(\mathbf{r}), & \text{if } \xi < \xi_b. \end{cases} \tag{22}$$

IV. ANALYTICAL SOLUTION FOR THE QUASI-HARMONIC DIELECTRIC MODEL

The major problem of employing the step-like dielectric model and the corresponding analytical solution (22) to calculate the self-polarization energy lies in the fact that it diverges at the ellipsoidal surface $\xi = \xi_b$. In order to overcome such mathematical divergence, a natural consideration is to introduce a thin transition layer of finite width in the ξ-direction, say 2δ, centered at $\xi = \xi_b$ with a continuous radial dielectric profile, say $\varepsilon(\xi)$, separating the two dielectric continua ε_i and ε_o, leading to a three-layer dielectric model, as shown in Fig. 2. For the inner layer of $\xi \leq \xi_b - \delta$, the dielectric constant takes the value ε_i, while for the outer layer of $\xi \geq \xi_b + \delta$, the dielectric constant takes the value ε_o. Between them, for the intermediate transition layer of $\xi_b - \delta < \xi < \xi_b + \delta$, one can choose any analytical and physically plausible continuous profile for $\varepsilon(\xi)$ to connect these two extreme values. Two natural choices of $\varepsilon(\xi)$ include the linear profile defined by

$$\varepsilon(\xi) = \begin{cases} \varepsilon_i, & \text{if } \xi \leq \xi_I, \\ \dfrac{\varepsilon_i + \varepsilon_o}{2} + \dfrac{\varepsilon_i - \varepsilon_o}{2\delta}\ (\xi_b - \xi), & \text{if } \xi_I < \xi < \xi_O, \\ \varepsilon_o, & \text{if } \xi \geq \xi_O, \end{cases} \tag{23}$$

and the cosine-like profile given by

$$\varepsilon(\xi) = \begin{cases} \varepsilon_i, & \text{if } \xi \le \xi_I, \\ \dfrac{\varepsilon_i + \varepsilon_o}{2} + \dfrac{\varepsilon_i - \varepsilon_o}{2} \cos\left(\dfrac{\xi - \xi_I}{2\delta}\pi\right), & \text{if } \xi_I < \xi < \xi_O, \\ \varepsilon_o, & \text{if } \xi \ge \xi_O, \end{cases} \tag{24}$$

respectively, where $\xi_I = \xi_b - \delta$ and $\xi_O = \xi_b + \delta$ represent the inner and the outer boundaries of the transition layer, respectively.

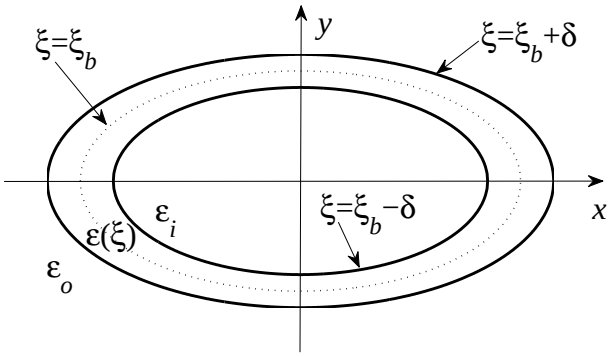

FIG. 2: Schematic illustration of a three-layer dielectric model: The inner layer ($\xi \le \xi_b - \delta$) has a dielectric constant of ε_i, while the outer layer ($\xi \ge \xi_b + \delta$) has a dielectric constant of ε_o. The intermediate transition layer ($\xi_b - \delta < \xi < \xi_b + \delta$) assumes a continuous dielectric permittivity profile $\varepsilon(\xi)$ that connects ε_i and ε_o. The graph shown represents the xy-cross section of the ellipsoid.

As indicated earlier, for general three-layer dielectric profiles $\varepsilon(\xi)$ including the linear and the cosine-like ones, it does not seem feasible to find an explicit analytical solution for the Poisson equation (1) since it is a second-order differential equation with a variable coefficient. However, an explicit analytical solution can be obtained for the following *quasi-harmonic* three-layer dielectric profile:

$$\varepsilon(\xi) = \begin{cases} \varepsilon_i, & \text{if } \xi \le \xi_I, \\ \left[\alpha + \beta F_0^1(\xi)\right]^2, & \text{if } \xi_I < \xi < \xi_O, \\ \varepsilon_o, & \text{if } \xi \ge \xi_O, \end{cases} \tag{25}$$

where

$$\alpha = \frac{c\sqrt{\varepsilon_o} - d\sqrt{\varepsilon_i}}{c - d} \quad \text{and} \quad \beta = \frac{\sqrt{\varepsilon_i} - \sqrt{\varepsilon_o}}{c - d}, \tag{26}$$

with

$$c = F_0^1(\xi_I) \quad \text{and} \quad d = F_0^1(\xi_O)\,. \tag{27}$$

The reason why $\varepsilon(\xi)$ defined in (25) is called "quasi-harmonic" is because it is not harmonic by itself but $\sqrt{\varepsilon(\xi)}$, being a linear combination of two harmonic eigen-functions $E_0^1(\xi) \equiv 1$ and $F_0^1(\xi)$, is harmonic. The three three-layer dielectric models mentioned so far together with the step-like model are illustrated in Fig. 3. Note that in terms of the Jacobi elliptic function sn(...), we have [15]

$$F_0^1(\xi) = \int_\xi^\infty \frac{\mathrm{d}\xi'}{\sqrt{(\xi'^2 - k^2)(\xi'^2 - h^2)}} = \frac{1}{k}\,\mathrm{sn}^{-1}\left(\frac{k}{\xi}, \frac{h}{k}\right), \tag{28}$$

Also note that

$$F_0^{1\prime}(\xi) = -\frac{1}{\sqrt{(\xi^2 - k^2)(\xi^2 - h^2)}}. \tag{29}$$

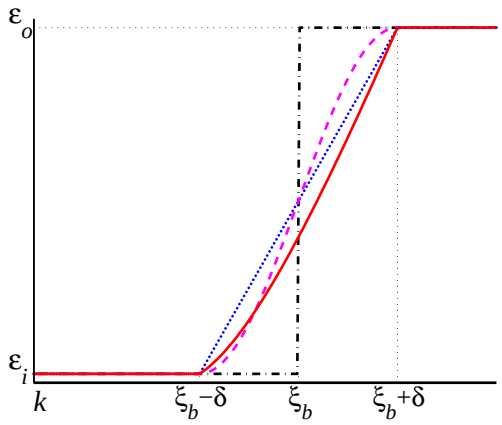

FIG. 3: (Color online) Illustration of several three-layer dielectric models together with the step-like model, assuming $\varepsilon_i < \varepsilon_o$. Dot-dashed line, the step-like model; dotted line, the linear model; dashed line, the cosine-like model; and solid line, the quasi-harmonic model. This particular graph is for $a = 4, b = 3, c = 2$, $\delta = 0.2$, $\varepsilon_i = 2$ and $\varepsilon_o = 80$.

Before we proceed, it should be emphasized that, while similar potential problems in the ellipsoidal geometry have been investigated in many different realms by many different researchers, and the basic techniques to be used in this paper are no different from those used to solve many other problems, to the best of the authors' knowledge, most of the works in the literature either assume the step-like dielectric profile or consider problems involving multiple *homogeneous* confocal ellipsoidal shells. In particular, we are unaware of any work

that considers the three-layer dielectric models in the ellipsoidal geometry. While there is nothing special about the linear and the cosine-like three-layer models, at present the quasi-harmonic dielectric model appears to be the only three-layer model such that the resulting Poisson equation (1) admits explicit analytical series solutions. Most importantly, as to be described in Section V, based on the proposed quasi-harmonic three-layer dielectric model, a *robust* numerical method can be developed that essentially can be used to solve the Poisson equation (1) with any radially dependent dielectric function.

The explicit analytical series solution to the Poisson equation (1) corresponding to the above quasi-harmonic dielectric model is easy to find. First, let us consider the case when the point charge e_s is located inside the inner layer ($\xi_s \leq \xi_I = \xi_b - \delta$). Accordingly, the Poisson equation (1) becomes

$$\nabla \cdot \varepsilon_i \nabla \Phi_i(\mathbf{r}, \mathbf{r}_s) = -4\pi e_s \delta(\mathbf{r} - \mathbf{r}_s), \qquad \text{if } \xi \leq \xi_I, \tag{30a}$$

$$\nabla \cdot \varepsilon(\xi) \nabla \Phi_t(\mathbf{r}, \mathbf{r}_s) = 0, \qquad \text{if } \xi_I < \xi < \xi_O, \tag{30b}$$

$$\Delta \Phi_o(\mathbf{r}, \mathbf{r}_s) = 0, \qquad \text{if } \xi \geq \xi_O, \tag{30c}$$

where Φ_i, Φ_t, and Φ_o stand for the electrostatic potential in the inner, the transition, and the outer layers, respectively.

At the two boundaries of the transition layer, the continuity of the potential and the normal flux requires that

$$\Phi_i|_{\xi=\xi_I} = \Phi_t|_{\xi=\xi_I} \quad \text{and} \quad \left.\frac{\partial \Phi_i}{\partial \xi}\right|_{\xi=\xi_I} = \left.\frac{\partial \Phi_t}{\partial \xi}\right|_{\xi=\xi_I}, \tag{31}$$

$$\Phi_o|_{\xi=\xi_O} = \Phi_t|_{\xi=\xi_O} \quad \text{and} \quad \left.\frac{\partial \Phi_o}{\partial \xi}\right|_{\xi=\xi_O} = \left.\frac{\partial \Phi_t}{\partial \xi}\right|_{\xi=\xi_O}. \tag{32}$$

The key in finding the analytical solution for the Poisson equation (1) corresponding to the quasi-harmonic model is the following important observation [10, 32].

Theorem 1 *If the variable coefficient $\varepsilon(\mathbf{r})$ in the quasi-harmonic equation*

$$\nabla \cdot [\varepsilon(\mathbf{r}) \nabla \phi(\mathbf{r})] = 0 \tag{33}$$

satisfies $\Delta \sqrt{\varepsilon(\mathbf{r})} = 0$, then

$$\Delta \left[\sqrt{\varepsilon(\mathbf{r})} \phi(\mathbf{r}) \right] = 0. \tag{34}$$

Similarly, if the variable coefficient $\varepsilon(\mathbf{r})$ in the quasi-elliptic equation

$$\nabla \cdot [\varepsilon(\mathbf{r})\nabla\phi(\mathbf{r})] = \rho(\mathbf{r}) \tag{35}$$

satisfies $\Delta\sqrt{\varepsilon(\mathbf{r})} = 0$, then

$$\Delta\left[\sqrt{\varepsilon(\mathbf{r})}\phi(\mathbf{r})\right] = \rho(\mathbf{r})/\sqrt{\varepsilon(\mathbf{r})}. \tag{36}$$

Since by construction, $\Delta\sqrt{\varepsilon(\xi)} = 0$ in the transition layer, the Poisson equation (30b) can be re-written as a Laplace equation

$$\Delta\left[\sqrt{\varepsilon(\xi)}\Phi_t(\mathbf{r},\mathbf{r}_s)\right] = 0, \tag{37}$$

whose solution $\sqrt{\varepsilon(\xi)}\Phi_t(\mathbf{r},\mathbf{r}_s)$ shall be expanded in terms of both the internal and the external harmonics. Consequently, the potential Φ_t can be expressed as

$$\Phi_t(\mathbf{r},\mathbf{r}_s) = \frac{e_s}{\sqrt{\varepsilon(\xi)}}\hat{\sum}\left[C_{np}\mathcal{E}_n^p(\mathbf{r}) + D_{np}\mathcal{F}_n^p(\mathbf{r})\right], \tag{38}$$

or, when the charge e_s is also located inside the transition layer, as

$$\Phi_t(\mathbf{r},\mathbf{r}_s) = \frac{e_s}{\sqrt{\varepsilon_s\varepsilon(\xi)}|\mathbf{r}-\mathbf{r}_s|} + \frac{e_s}{\sqrt{\varepsilon(\xi)}}\hat{\sum}\left[C_{np}\mathcal{E}_n^p(\mathbf{r}) + D_{np}\mathcal{F}_n^p(\mathbf{r})\right], \tag{39}$$

where $\varepsilon_s = \varepsilon(\xi_s)$, and C_{np} and D_{np} are undetermined constant expansion coefficients.

For the purpose of simplifying mathematical formulations, now we actually write the potentials in the three layers as

$$\Phi_o(\mathbf{r},\mathbf{r}_s) = \frac{e_s}{\sqrt{\varepsilon_i\varepsilon_o}}\hat{\sum}A_{np}^{(1)}\cdot\mathcal{K}_{np}\mathcal{E}_n^p(\mathbf{r}_s)\mathcal{F}_n^p(\mathbf{r}), \tag{40a}$$

$$\Phi_i(\mathbf{r},\mathbf{r}_s) = \frac{e_s}{\varepsilon_i|\mathbf{r}-\mathbf{r}_s|} + \frac{e_s}{\varepsilon_i}\hat{\sum}B_{np}^{(1)}\cdot\mathcal{K}_{np}\mathcal{E}_n^p(\mathbf{r}_s)\mathcal{E}_n^p(\mathbf{r}), \tag{40b}$$

$$\Phi_t(\mathbf{r},\mathbf{r}_s) = \frac{e_s}{\sqrt{\varepsilon_i\varepsilon(\xi)}}\hat{\sum}\mathcal{K}_{np}\mathcal{E}_n^p(\mathbf{r}_s)\left[C_{np}^{(1)}\mathcal{E}_n^p(\mathbf{r}) + D_{np}^{(1)}\mathcal{F}_n^p(\mathbf{r})\right]. \tag{40c}$$

Here, the constant expansion coefficients $A_{np}^{(1)}, B_{np}^{(1)}, C_{np}^{(1)}$, and $D_{np}^{(1)}$ can be determined by the boundary conditions (31)-(32), together with the orthogonality relation (9), and the expansion of the reciprocal distance (11). Omitting all details, we have

$$\mathbf{M}\times\begin{pmatrix} A_{np}^{(1)} \\ B_{np}^{(1)} \\ C_{np}^{(1)} \\ D_{np}^{(1)} \end{pmatrix} = \begin{pmatrix} -F_n^p(\xi_I) \\ 0 \\ -F_n^{p\prime}(\xi_I) \\ 0 \end{pmatrix}, \tag{41}$$

where

$$\mathbf{M}=\begin{bmatrix} 0, & E_n^p(\xi_I), & -E_n^p(\xi_I), & -F_n^p(\xi_I) \\ F_n^p(\xi_O), & 0, & -E_n^p(\xi_O), & -F_n^p(\xi_O) \\ 0, & E_n^{p\prime}(\xi_I), & -E_n^{p\prime}(\xi_I)+\dfrac{\beta F_0^{1\prime}(\xi_I)}{\sqrt{\varepsilon_i}}E_n^p(\xi_I), & -F_n^{p\prime}(\xi_I)+\dfrac{\beta F_0^{1\prime}(\xi_I)}{\sqrt{\varepsilon_i}}F_n^p(\xi_I) \\ F_n^{p\prime}(\xi_O), & 0, & -E_n^{p\prime}(\xi_O)+\dfrac{\beta F_0^{1\prime}(\xi_O)}{\sqrt{\varepsilon_o}}E_n^p(\xi_O), & -F_n^{p\prime}(\xi_O)+\dfrac{\beta F_0^{1\prime}(\xi_O)}{\sqrt{\varepsilon_o}}F_n^p(\xi_O) \end{bmatrix}. \tag{42}$$

Similarly, if e_s is located inside the outer layer ($\xi_s \geq \xi_O = \xi_b + \delta$), we can write

$$\Phi_o(\mathbf{r},\mathbf{r}_s)=\frac{e_s}{\varepsilon_o|\mathbf{r}-\mathbf{r}_\mathrm{s}|}+\frac{e_s}{\varepsilon_o}\hat{\sum}A_{np}^{(2)}\cdot\mathcal{K}_{np}\mathcal{F}_n^p(\mathbf{r}_s)\mathcal{F}_n^p(\mathbf{r}), \tag{43a}$$

$$\Phi_i(\mathbf{r},\mathbf{r}_s)=\frac{e_s}{\sqrt{\varepsilon_o\varepsilon_i}}\hat{\sum}B_{np}^{(2)}\cdot\mathcal{K}_{np}\mathcal{F}_n^p(\mathbf{r}_s)\mathcal{E}_n^p(\mathbf{r}), \tag{43b}$$

$$\Phi_t(\mathbf{r},\mathbf{r}_s)=\frac{e_s}{\sqrt{\varepsilon_o\varepsilon(\xi)}}\hat{\sum}\mathcal{K}_{np}\mathcal{F}_n^p(\mathbf{r}_s)\left[C_{np}^{(2)}\mathcal{E}_n^p(\mathbf{r})+D_{np}^{(2)}\mathcal{F}_n^p(\mathbf{r})\right], \tag{43c}$$

where the constant expansion coefficients $A_{np}^{(2)}, B_{np}^{(2)}, C_{np}^{(2)}$, and $D_{np}^{(2)}$ can be calculated by

$$\mathbf{M}\times\begin{pmatrix} A_{np}^{(2)} \\ B_{np}^{(2)} \\ C_{np}^{(2)} \\ D_{np}^{(2)} \end{pmatrix}=\begin{pmatrix} 0 \\ -E_n^p(\xi_O) \\ 0 \\ -E_n^{p\prime}(\xi_O) \end{pmatrix}. \tag{44}$$

Finally, when e_s is located inside the transition layer ($\xi_I < \xi_s < \xi_O$), we can write

$$\Phi_o(\mathbf{r},\mathbf{r}_s)=\frac{e_s}{\sqrt{\varepsilon_s\varepsilon_o}}\hat{\sum}\mathcal{K}_{np}\left[A_{np}^{(3)}\mathcal{F}_n^p(\mathbf{r}_s)+A_{np}^{(4)}\mathcal{E}_n^p(\mathbf{r}_s)\right]\mathcal{F}_n^p(\mathbf{r}), \tag{45a}$$

$$\Phi_i(\mathbf{r},\mathbf{r}_s)=\frac{e_s}{\sqrt{\varepsilon_s\varepsilon_i}}\hat{\sum}\mathcal{K}_{np}\left[B_{np}^{(3)}\mathcal{F}_n^p(\mathbf{r}_s)+B_{np}^{(4)}\mathcal{E}_n^p(\mathbf{r}_s)\right]\mathcal{E}_n^p(\mathbf{r}), \tag{45b}$$

$$\begin{aligned}\Phi_t(\mathbf{r},\mathbf{r}_s)=&\frac{e_s}{\sqrt{\varepsilon_s\varepsilon(\xi)}|\mathbf{r}-\mathbf{r}_s|}+\frac{e_s}{\sqrt{\varepsilon_s\varepsilon(\xi)}}\hat{\sum}\mathcal{K}_{np}\left[\left(C_{np}^{(3)}\mathcal{F}_n^p(\mathbf{r}_s)\right.\right.\\ &\left.\left.+C_{np}^{(4)}\mathcal{E}_n^p(\mathbf{r}_s)\right)\mathcal{E}_n^p(\mathbf{r})+\left(D_{np}^{(3)}\mathcal{F}_n^p(\mathbf{r}_s)+D_{np}^{(4)}\mathcal{E}_n^p(\mathbf{r}_s)\right)\mathcal{F}_n^p(\mathbf{r})\right].\end{aligned} \tag{45c}$$

Here, the constant expansion coefficients $A_{np}^{(3)}, B_{np}^{(3)}, C_{np}^{(3)}$, and $D_{np}^{(3)}$ are determined by

$$\mathbf{M}\times\begin{pmatrix} A_{np}^{(3)} \\ B_{np}^{(3)} \\ C_{np}^{(3)} \\ D_{np}^{(3)} \end{pmatrix}=\begin{pmatrix} E_n^p(\xi_I) \\ 0 \\ E_n^{p\prime}(\xi_I)-\dfrac{\beta F_0^{1\prime}(\xi_I)}{\sqrt{\varepsilon_i}}E_n^p(\xi_I) \\ 0 \end{pmatrix}, \tag{46}$$

while $A_{np}^{(4)}, B_{np}^{(4)}, C_{np}^{(4)}$, and $D_{np}^{(4)}$ are determined by

$$\mathbf{M} \times \begin{pmatrix} A_{np}^{(4)} \\ B_{np}^{(4)} \\ C_{np}^{(4)} \\ D_{np}^{(4)} \end{pmatrix} = \begin{pmatrix} 0 \\ F_n^p(\xi_O) \\ 0 \\ F_n^{p\prime}(\xi_O) - \dfrac{\beta F_0^{1\prime}(\xi_O)}{\sqrt{\varepsilon_o}} F_n^p(\xi_O) \end{pmatrix}. \tag{47}$$

Likely, it should be mentioned that in the above equations, all constant expansion coefficients depend only on the two ellipsoidal boundaries $\xi = \xi_I$ and $\xi = \xi_O$ of the transition layer as well as the dielectric mismatch ratio $\varepsilon_r = \varepsilon_i/\varepsilon_o$. Therefore, once the width of the transition layer is chosen, these coefficients have to be calculated only once even when there are many charges present and they move over time.

The practical implementation of the above analytical series solution additionally requires truncating the infinite summation at a finite n value, say N, which could be very large in order to reach convergence or high accuracy. Also, the magnitude of the Lam*é* functions may increase exponentially with the argument ξ and easily exceed the capacity of a computer especially when their orders are high. Therefore, to avoid potential overflow and computer cutoff errors, we further carry out more convenient rewritings of the previous solution so that the matrices of the resulting systems for the expansion coefficients involve only the ratios of the Lam*é* functions and the logarithmic derivatives of these functions. To this end, in addition to (14) and (15), we let

$$\gamma_{np} = u_{np}(\xi_I) v_{np}(\xi_O). \tag{48}$$

Then, when the charge e_s is located inside the inner layer, the potentials in the three layers are re-written as

$$\Phi_o(\mathbf{r}, \mathbf{r}_s) = \frac{e_s}{\sqrt{\varepsilon_i \varepsilon_o}} \hat{\sum} A_{np}^{(1)} \cdot \mathcal{K}_{np} \mathcal{E}_n^p(\mathbf{r}_s) \mathcal{F}_n^p(\mathbf{r}), \tag{49a}$$

$$\Phi_i(\mathbf{r}, \mathbf{r}_s) = \frac{e_s}{\varepsilon_i |\mathbf{r} - \mathbf{r}_s|} + \frac{e_s}{\varepsilon_i} \hat{\sum} B_{np}^{(1)} \cdot v_{np}(\xi_I) \mathcal{K}_{np} \mathcal{E}_n^p(\mathbf{r}_s) \mathcal{E}_n^p(\mathbf{r}), \tag{49b}$$

$$\Phi_t(\mathbf{r}, \mathbf{r}_s) = \frac{e_s}{\sqrt{\varepsilon_i \varepsilon(\xi)}} \hat{\sum} \mathcal{K}_{np} \mathcal{E}_n^p(\mathbf{r}_s) \left[C_{np}^{(1)} v_{np}(\xi_O) \mathcal{E}_n^p(\mathbf{r}) + D_{np}^{(1)} \mathcal{F}_n^p(\mathbf{r}) \right], \tag{49c}$$

where the expansion coefficients $A_{np}^{(1)}, B_{np}^{(1)}, C_{np}^{(1)}$, and $D_{np}^{(1)}$ are now calculated by

$$\mathbf{M}^{(1)} \times \begin{pmatrix} A_{np}^{(1)} \\ B_{np}^{(1)} \\ C_{np}^{(1)} \\ D_{np}^{(1)} \end{pmatrix} = \begin{pmatrix} -1 \\ 0 \\ -\widetilde{F_n^p}(\xi_I) \\ 0 \end{pmatrix}, \tag{50}$$

with

$$\mathbf{M}^{(1)} = \begin{bmatrix} 0, & 1, & -\gamma_{np}, & -1 \\ 1, & 0, & -1, & -1 \\ 0, & \widetilde{E_n^p}(\xi_I), & \left[-\widetilde{E_n^p}(\xi_I) + \dfrac{\beta F_0^{1\prime}(\xi_I)}{\sqrt{\varepsilon_i}}\right]\gamma_{np}, & -\widetilde{F_n^p}(\xi_I) + \dfrac{\beta F_0^{1\prime}(\xi_I)}{\sqrt{\varepsilon_i}} \\ \widetilde{F_n^p}(\xi_O), & 0, & -\widetilde{E_n^p}(\xi_O) + \dfrac{\beta F_0^{1\prime}(\xi_O)}{\sqrt{\varepsilon_o}}, & -\widetilde{F_n^p}(\xi_O) + \dfrac{\beta F_0^{1\prime}(\xi_O)}{\sqrt{\varepsilon_o}} \end{bmatrix}. \tag{51}$$

Similarly, when the charge e_s is located inside the outer layer, the potentials are re-written as

$$\Phi_o(\mathbf{r}, \mathbf{r}_s) = \frac{e_s}{\varepsilon_o|\mathbf{r} - \mathbf{r}_s|} + \frac{e_s}{\varepsilon_o}\hat{\sum} A_{np}^{(2)} \cdot u_{np}(\xi_O)\mathcal{K}_{np}\mathcal{F}_n^p(\mathbf{r}_s)\mathcal{F}_n^p(\mathbf{r}), \tag{52a}$$

$$\Phi_i(\mathbf{r}, \mathbf{r}_s) = \frac{e_s}{\sqrt{\varepsilon_o\varepsilon_i}}\hat{\sum} B_{np}^{(2)} \cdot \mathcal{K}_{np}\mathcal{F}_n^p(\mathbf{r}_s)\mathcal{E}_n^p(\mathbf{r}), \tag{52b}$$

$$\Phi_t(\mathbf{r}, \mathbf{r}_s) = \frac{e_s}{\sqrt{\varepsilon_o\varepsilon(\xi)}}\hat{\sum} \mathcal{K}_{np}\mathcal{F}_n^p(\mathbf{r}_s)\left[C_{np}^{(2)}\mathcal{E}_n^p(\mathbf{r}) + D_{np}^{(2)}u_{np}(\xi_I)\mathcal{F}_n^p(\mathbf{r})\right], \tag{52c}$$

where the expansion coefficients $A_{np}^{(2)}, B_{np}^{(2)}, C_{np}^{(2)}$, and $D_{np}^{(2)}$ are now determined by

$$\mathbf{M}^{(2)} \times \begin{pmatrix} A_{np}^{(2)} \\ B_{np}^{(2)} \\ C_{np}^{(2)} \\ D_{np}^{(2)} \end{pmatrix} = \begin{pmatrix} 0 \\ -1 \\ 0 \\ -\widetilde{E_n^p}(\xi_O) \end{pmatrix}, \tag{53}$$

with

$$\mathbf{M}^{(2)} = \begin{bmatrix} 0, & 1, & -1, & -1 \\ 1, & 0, & -1, & -\gamma_{np} \\ 0, & \widetilde{E_n^p}(\xi_I), & -\widetilde{E_n^p}(\xi_I) + \dfrac{\beta F_0^{1\prime}(\xi_I)}{\sqrt{\varepsilon_i}}, & -\widetilde{F_n^p}(\xi_I) + \dfrac{\beta F_0^{1\prime}(\xi_I)}{\sqrt{\varepsilon_i}} \\ \widetilde{F_n^p}(\xi_O), & 0, & -\widetilde{E_n^p}(\xi_O) + \dfrac{\beta F_0^{1\prime}(\xi_O)}{\sqrt{\varepsilon_o}}, & \left[-\widetilde{F_n^p}(\xi_O) + \dfrac{\beta F_0^{1\prime}(\xi_O)}{\sqrt{\varepsilon_o}}\right]\gamma_{np} \end{bmatrix}. \tag{54}$$

Finally, when the charge e_s is located inside the transition layer, we can write

$$\Phi_o(\mathbf{r},\mathbf{r}_s) = \frac{e_s}{\sqrt{\varepsilon_s\varepsilon_o}}\hat{\sum}\mathcal{K}_{np}\left[A_{np}^{(3)}u_{np}(\xi_I)\mathcal{F}_n^p(\mathbf{r}_s)+A_{np}^{(4)}\mathcal{E}_n^p(\mathbf{r}_s)\right]\mathcal{F}_n^p(\mathbf{r}), \tag{55a}$$

$$\Phi_i(\mathbf{r},\mathbf{r}_s) = \frac{e_s}{\sqrt{\varepsilon_s\varepsilon_i}}\hat{\sum}\mathcal{K}_{np}\left[B_{np}^{(3)}\mathcal{F}_n^p(\mathbf{r}_s)+B_{np}^{(4)}v_{np}(\xi_O)\mathcal{E}_n^p(\mathbf{r}_s)\right]\mathcal{E}_n^p(\mathbf{r}), \tag{55b}$$

$$\begin{aligned}\Phi_t(\mathbf{r},\mathbf{r}_s) =& \frac{e_s}{\sqrt{\varepsilon_s\varepsilon(\xi)}|\mathbf{r}-\mathbf{r}_s|}+\frac{e_s}{\sqrt{\varepsilon_s\varepsilon(\xi)}}\hat{\sum}\left\{\mathcal{K}_{np}\right.\\ &\times\left[\left(C_{np}^{(3)}\gamma_{np}\mathcal{F}_n^p(\mathbf{r}_s)+C_{np}^{(4)}v_{np}(\xi_O)\mathcal{E}_n^p(\mathbf{r}_s)\right)\mathcal{E}_n^p(\mathbf{r})\right.\\ &\left.\left.+\left(D_{np}^{(3)}u_{np}(\xi_I)\mathcal{F}_n^p(\mathbf{r}_s)+D_{np}^{(4)}\gamma_{np}\mathcal{E}_n^p(\mathbf{r}_s)\right)\mathcal{F}_n^p(\mathbf{r})\right]\right\}.\end{aligned} \tag{55c}$$

Here, the expansion coefficients $A_{np}^{(3)}, B_{np}^{(3)}, C_{np}^{(3)}$, and $D_{np}^{(3)}$ are now determined by

$$\mathbf{M}^{(1)}\times\begin{pmatrix}A_{np}^{(3)}\\ B_{np}^{(3)}\\ C_{np}^{(3)}\\ D_{np}^{(3)}\end{pmatrix}=\begin{pmatrix}1\\ 0\\ \widetilde{E_n^p}(\xi_I)-\dfrac{\beta F_0^{1\prime}(\xi_I)}{\sqrt{\varepsilon_i}}\\ 0\end{pmatrix}, \tag{56}$$

while the expansion coefficients $A_{np}^{(4)}, B_{np}^{(4)}, C_{np}^{(4)}$, and $D_{np}^{(4)}$ are now determined by

$$\mathbf{M}^{(2)}\times\begin{pmatrix}A_{np}^{(4)}\\ B_{np}^{(4)}\\ C_{np}^{(4)}\\ D_{np}^{(4)}\end{pmatrix}=\begin{pmatrix}0\\ 1\\ 0\\ \widetilde{F_n^p}(\xi_O)-\dfrac{\beta F_0^{1\prime}(\xi_O)}{\sqrt{\varepsilon_o}}\end{pmatrix}. \tag{57}$$

Accordingly, from (49b), (52a) and (55c), the self-polarization potential energy of a charged particle e at the location $\mathbf{r}$ can be arrived at as follows.

$$V_s(\mathbf{r})=\begin{cases}\dfrac{e^2}{2\varepsilon_o}\hat{\sum}A_{np}^{(2)}\cdot u_{np}(\xi_O)\mathcal{K}_{np}\mathcal{F}_n^{p2}(\mathbf{r}), & \text{if } \xi\geq\xi_O,\\ \dfrac{e^2}{2\varepsilon_i}\hat{\sum}B_{np}^{(1)}\cdot v_{np}(\xi_I)\mathcal{K}_{np}\mathcal{E}_n^{p2}(\mathbf{r}), & \text{if } \xi\leq\xi_I,\\ \dfrac{e^2}{2\varepsilon(\xi)}\hat{\sum}\mathcal{K}_{np}\left[\gamma_{np}\left(C_{np}^{(3)}+D_{np}^{(4)}\right)\mathcal{E}_n^p(\mathbf{r})\mathcal{F}_n^p(\mathbf{r})\right.\\ \qquad\left.+v_{np}(\xi_O)C_{np}^{(4)}\mathcal{E}_n^{p2}(\mathbf{r})+u_{np}(\xi_I)D_{np}^{(3)}\mathcal{F}_n^{p2}(\mathbf{r})\right], & \text{if } \xi_I<\xi<\xi_O.\end{cases} \tag{58}$$

V. NUMERICAL METHOD FOR GENERAL THREE-LAYER DIELECTRIC MODELS

The Poisson equation (1) corresponding to a general three-layer dielectric model does not admit an easy explicit analytical solution and thus needs to be solved numerically. One could develop a numerical procedure similar to that proposed by Bolcatto *et al.* in [4] for the spherical geometry. First, the transition layer is subdivided into multiple sublayers, and then in each one of them the select dielectric function is approximated by a constant value such as the mean value of the dielectric function in this sublayer. As the result, the original continuous radial dielectric profile is approximated by a piecewise constant one, and consequently, the original Poisson equation with the continuous radial dielectric profile reduces to one in layered dielectric ellipsoids, whose solution can then be found in the same way as for the Poisson equation in layered spheres [4, 13, 33–36]. However, this approach has a fundamental limitation: as it discretizes a continuous dielectric function $\varepsilon(\xi)$ into a piecewise constant one within the transition layer, and the ultimate effect of such discretization is to approximate a continuous self-polarization potential energy by one with divergence at every interface between those sublayers, new numerical divergence emerges.

Therefore, as in [1, 11], we employ an ideally only slightly more complicated but computationally much more robust numerical procedure. Basically, the procedure first still divides the transition layer, $\xi_b - \delta < \xi < \xi_b + \delta$, into multiple, say $L-1$, sublayers, $[\xi_{l-1}, \xi_l], l = 1, 2, \ldots, L-1$, with $\xi_0 = \xi_b - \delta$ and $\xi_{L-1} = \xi_b + \delta$. For convenience, also set $\xi_{-1} = k$ and $\xi_L = \infty$. For each index $l = -1, 0, \ldots, L$, denote by e_l the dielectric constant at $\xi = \xi_l$, namely, $e_l = \varepsilon(\xi_l)$. Note that $e_{-1} = e_0 = \varepsilon_i$ and $e_{L-1} = e_L = \varepsilon_o$. Then in each sublayer $[\xi_{l-1}, \xi_l]$, $l = 0, 1, \ldots, L$, the dielectric function $\varepsilon(\xi)$ is approximated by a quasi-harmonic one of the form (25) that connects e_{l-1} and e_l, namely, by

$$\varepsilon_l(\xi) = \left[\alpha_l + \beta_l F_0^1(\xi)\right]^2, \quad \xi_{l-1} \le \xi \le \xi_l, \quad l = 0, 1, \ldots, L,$$

where

$$\alpha_l = \frac{c_l\sqrt{e_l} - d_l\sqrt{e_{l-1}}}{c_l - d_l} \quad \text{and} \quad \beta_l = \frac{\sqrt{e_{l-1}} - \sqrt{e_l}}{c_l - d_l}, \tag{59}$$

with

$$c_l = F_0^1\left(\xi_{l-1}\right) \quad \text{and} \quad d_l = F_0^1\left(\xi_l\right). \tag{60}$$

Note that now the approximating dielectric profile remains continuous. As the result, the

self-polarization potential energy has no numerical divergence, and, as the number of sublayers used to discretize the transition layer increases, the numerical solution shall converge to the exact solution of the Poisson equation.

Next, in each sublayer the solution of the Poisson equation is expressed as

$$\Phi_l(\mathbf{r},\mathbf{r}_s)=\frac{e_s}{\sqrt{\varepsilon_l(\xi)}}\hat{\sum}\left[C_{np}^{(l)}\mathcal{E}_n^p(\mathbf{r})+D_{np}^{(l)}\mathcal{F}_n^p(\mathbf{r})\right],\quad \text{if}\quad \xi_{l-1}\le\xi\le\xi_l. \tag{61}$$

Finally, by using a recursive method in analogy to the analysis of transmission lines [1, 4, 11, 13, 33–36], those constant expansion coefficients $C_{np}^{(l)}$ and $D_{np}^{(l)}$ can be determined from the following interface conditions for $l=1,2,\ldots,L$,

$$\Phi_{l-1}\big|_{\xi=\xi_{l-1}^-}=\Phi_l\big|_{\xi=\xi_{l-1}^+}\quad\text{and}\quad \left.\frac{\partial\Phi_{l-1}}{\partial\xi}\right|_{\xi=\xi_{l-1}^-}=\left.\frac{\partial\Phi_l}{\partial\xi}\right|_{\xi=\xi_{l-1}^+}.$$

As the result of the above procedure, explicit numerical formulas for solving the Poisson equation (1) for general three-layer dielectric models can be obtained. More precisely, the generalized Coulomb potential at a point $\mathbf{r}$ in the l-th sublayer due to a point charge e_s at another point $\mathbf{r}_s$ in the k-th [37] sublayer can be calculated by

$$\Phi_{lk}(\mathbf{r},\mathbf{r}_s)=\frac{e_s}{\sqrt{\varepsilon_l(\xi)\varepsilon_k(\xi_s)}}\hat{\sum}\mathcal{K}_{np}Y_n^p(\mu_s,\nu_s)Y_n^p(\mu,\nu)\times\frac{W_{np,lk}(\xi,\xi_s)}{(1-p_{np,kk}q_{np,kk})}, \tag{62}$$

where the functions $W_{np,lk}(\xi,\xi_s)$ are given by

$$W_{np,lk}(\xi,\xi_s)=\left[p_{np,kk}E_n^p(\xi_>)+F_n^p(\xi_>)\right]\left[E_n^p(\xi_<)+q_{np,lk}F_n^p(\xi_<)\right]\hat{C}_{np}^l \tag{63}$$

if $l<k$,

$$W_{np,lk}(\xi,\xi_s)=\left[p_{np,kk}E_n^p(\xi_>)+F_n^p(\xi_>)\right]\left[E_n^p(\xi_<)+q_{np,kk}F_n^p(\xi_<)\right] \tag{64}$$

for $l=k$, and

$$W_{np,lk}(\xi,\xi_s)=\left[p_{np,lk}E_n^p(\xi_>)+F_n^p(\xi_>)\right]\left[E_n^p(\xi_<)+q_{np,kk}F_n^p(\xi_<)\right]\tilde{D}_{np}^l \tag{65}$$

when $l>k$. Here, $\xi_<$ ($\xi_>$) is the smaller (greater) between ξ and ξ_s,

$$p_{np,lk}=T_{np}^k v_{np}(\xi_l)\quad\text{and}\quad q_{np,lk}=R_{np}^{k-1}u_{np}(\xi_{l-1}), \tag{66}$$

[37] To be consistent with previous publications, here we have used k as an index although it is also used to represent $\sqrt{a^2-c^2}$ in the paper.

and

$$\hat{C}_{np}^{l} = \prod_{j=l}^{k-1} \frac{T_{np,j+1}}{1 - R_{np,j+1} R_{np}^{j-1} \gamma_{np,j}}, \tag{67a}$$

$$\tilde{D}_{np}^{l} = \prod_{j=k+1}^{l} \frac{T_{np,j}}{1 - R_{np,j} T_{np}^{j} \gamma_{np,j}}. \tag{67b}$$

In the previous formulations, $\gamma_{np,l} = u_{np}(\xi_{l-1}) v_{np}(\xi_l)$, $l = 0, 1, \cdots, L$. In particular, $\gamma_{np,0} = \gamma_{np,L} = 0$. $R_{np,l}$ and $T_{np,l}$, identified as the interface parameters associated to the interface $\xi = \xi_{l-1}$, are given by

$$R_{np,l} = (\beta_l - \beta_{l-1}) F_0^{1'}(\xi_{l-1}) / \Delta_{np,l}, \tag{68a}$$

$$T_{np,l} = \sqrt{e_{l-1}} \left[\widetilde{F_n^p}(\xi_{l-1}) - \widetilde{E_n^p}(\xi_{l-1}) \right] / \Delta_{np,l}, \tag{68b}$$

$$\Delta_{np,l} = \sqrt{e_{l-1}} \left[\widetilde{F_n^p}(\xi_{l-1}) - \widetilde{E_n^p}(\xi_{l-1}) \right] - (\beta_l - \beta_{l-1}) F_0^{1'}(\xi_{l-1}). \tag{68c}$$

On the other hand, R_{np}^{l} and T_{np}^{l}, identified as the interface reflection and the transmission coefficients associated to the interface $\xi = \xi_{l-1}$, are given through the following recursive expressions

$$R_{np}^{l-1} = R_{np,l} + \frac{T_{np,l}^2 R_{np}^{l-2} \gamma_{np,l-1}}{1 - R_{np,l} R_{np}^{l-2} \gamma_{np,l-1}} \quad \text{with} \quad R_{np}^{-1} = 0, \tag{69}$$

$$T_{np}^{l-1} = R_{np,l} + \frac{T_{np,l}^2 T_{np}^{l} \gamma_{np,l}}{1 - R_{np,l} T_{np}^{l} \gamma_{np,l}} \quad \text{with} \quad T_{np}^{L} = 0. \tag{70}$$

Consequently, the self-polarization energy of a charged particle e at a point $\mathbf{r}$ in the l-th sublayer where $0 \leq l \leq L$, denoted by $V_s^l(\mathbf{r})$, can be calculated by $V_s^l(\mathbf{r}) = \frac{1}{2} e \Phi_{ll}(\mathbf{r}, \mathbf{r})$. In accordance with (62), the self-energy reads

$$\begin{aligned} V_s^l(\mathbf{r}) = & \frac{e^2}{2\varepsilon_l(\xi)} \hat{\sum} \left\{ \frac{\mathcal{K}_{np} E_n^{p2}(\mu) E_n^{p2}(\nu)}{(1 - p_{np,ll} q_{np,ll})} \right. \\ & \left. \times \left[p_{np,ll} E_n^{p2}(\xi) + p_{np,ll} q_{np,ll} E_n^{p}(\xi) F_n^{p}(\xi) + q_{np,ll} F_n^{p2}(\xi) \right] \right\}. \end{aligned} \tag{71}$$

VI. ILLUSTRATIVE NUMERICAL EXPERIMENTS

In this section, we apply the analytical solution for the proposed quasi-harmonic dielectric model as well as the proposed numerical solution for general three-layer dielectric models to the calculation of the self-polarization energy of a tri-axial ellipsoidal quantum dot (QD), in which the dielectric constant inside the dot is typically higher than that of the surrounding

matrix. In particular, we consider the ellipsoidal QD given by $x^2/a^2 + y^2/b^2 + z^2/c^2 = 1$ with $a = 20$ Å, $b = 15$ Å, $c = 10$ Å and $\varepsilon_i = 12.6$ (GaAs), and assume that it is embedded in vacuum ($\varepsilon_o = 1$). In all simulations, the imposed upper limit of n is set to $N = 100$. Unless otherwise specified, all analytical results and illustrative plots are based on the calculation of the self-polarization energies of 1000 unit charges (in atomic unit) uniformly distributed (in terms of the ξ-dependent distance) along the line segment OP with two endpoints $O = (0, 0, 0)$ and $P = (26, 24, 18)$. Furthermore, when the numerical solution is involved, the number of sublayers used to discretize the transition layer is set to $L = 1000$.

A. Self-energy for the step-like dielectric model

Figure 4(a) shows the self-polarization energy profile and Fig. 4(b) shows the contour graph of the electrostatic potential distribution on the x-y plane due to a unit point charge inside the QD at the point $\mathbf{r}_s = (10, 7.5, 5)$, respectively, corresponding to the simple step-like model. It is well known that under the step-like model, when the source charge is placed in the region with a lower dielectric constant, the induced charges have the opposite sign as the source charge and then the interaction between the source and the induced charges is attractive. On the contrary, if the source charge is located in the region with a higher dielectric constant, the induced charges have the same sign as the source charge and then the interaction is repulsive. Here $\varepsilon_i > \varepsilon_o$, so as shown in Fig. 4(a), the self-polarization energy is positive inside the dot but negative outside. Moreover, as the source charge moves to the QD boundary, the self-energy increases rapidly in magnitude, leading to divergence at the QD boundary. On the other hand, Fig. 4(b) clearly shows that, under the step-like model, the resulting electrostatic potential is continuous but its normal derivative is discontinuous across the boundary, as required by the boundary condition (18).

B. Self-energy for the quasi-harmonic dielectric model

Figure 5(a) shows the self-polarization energy profile and Fig. 5(b) shows the contour graph of the electrostatic potential distribution on the x-y plane due to a unit point charge inside the QD at the point $\mathbf{r}_s = (10, 7.5, 5)$, respectively, corresponding to the proposed quasi-harmonic model with $\delta = 2$ Å. As can be seen from Fig. 5(a), under the quasi-harmonic

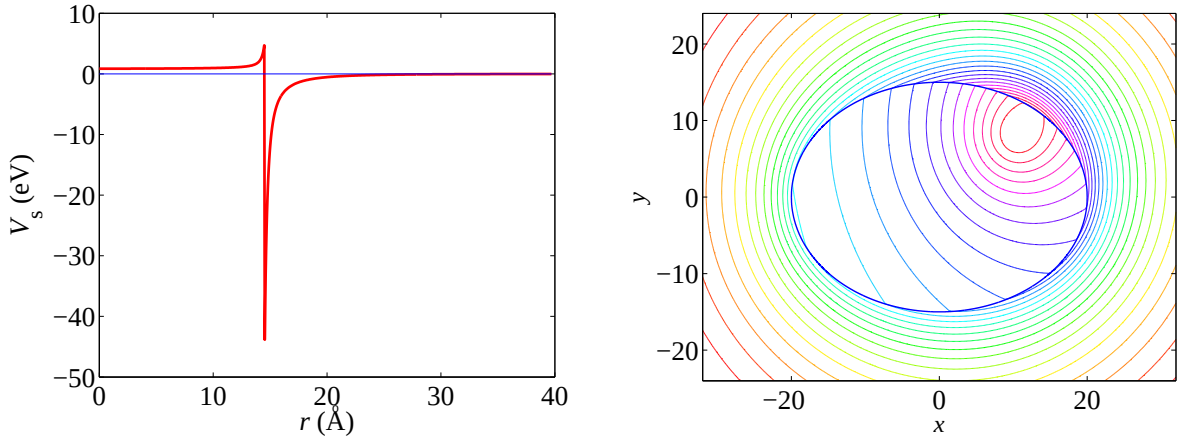

(a) (b)

FIG. 4: (Color online) (a) Self-polarization energy V_s of unit charges along the line segment OP, and (b) the contour graph of the electrostatic potential distribution on the x-y plane due to a unit point charge at $\mathbf{r}_s = (10, 7.5, 5)$ inside the ellipsoidal QD, corresponding to the step-like model.

model, as the source charge moves from the center to the outside of the dot along the line segment OP, the self-polarization energy first increases and reaches its maximum value at the inner boundary of the transition layer. Then, it gradually decreases from positive to negative (but with higher and higher rate) within the transition layer. Once the self-energy reaches its minimum value at the outer boundary of the transition layer, it gradually increases to zero (but with lower and lower rate). As a result, the mathematical divergence present in the step-like model is overcome. Also, although the quasi-harmonic dielectric model leads to singularity in the self-polarization potential energy at both boundaries of the transition layer, precisely where the derivative of $\varepsilon(\mathbf{r})$ is discontinuous, fortunately this kind of singularity is integrable. On the other hand, Fig. 5(b) clearly shows that, under the quasi-harmonic model, both the electrostatic potential and its normal derivative are continuous across the boundaries of the transition layer, as required by the boundary conditions (31) and (32).

Figure 6 shows the self-polarization energy profile of unit charges along the line segment OP corresponding to the quasi-harmonic model with several different thickness of the transition layer, namely, $\delta = 2$ Å, 1 Å, and 0.5 Å, respectively. Clearly, it is observed that, as the transition layer decreases in size, the self-polarization energy given by the analytical solution for the quasi-harmonic model reduces to that for the step-like model.

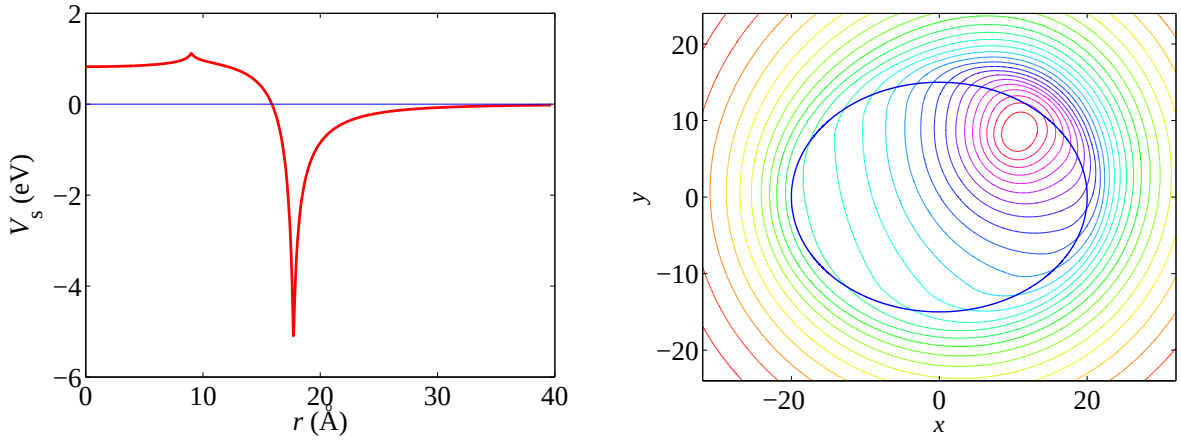

(a) (b)

FIG. 5: (Color online) (a) Self-polarization energy V_s of unit charges along the line segment OP, and (b) the contour graph of the electrostatic potential distribution on the x-y plane due to a unit point charge at $\mathbf{r}_s = (10, 7.5, 5)$ inside the ellipsoidal QD, corresponding to the quasi-harmonic model with $\delta = 2$ Å. Note that in this case, $\mathbf{r}_s = (10, 7.5, 5)$ is actually inside the transition layer.

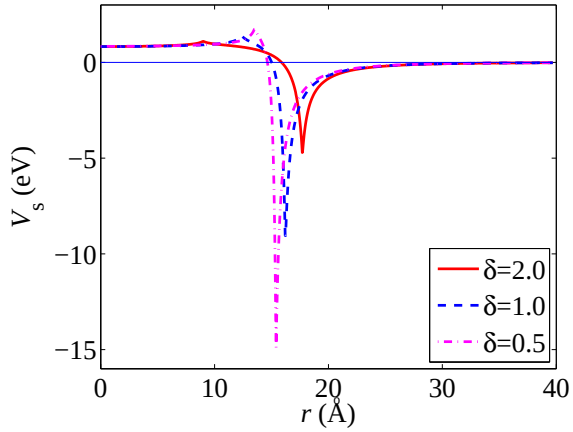

FIG. 6: (Color online) Self-polarization energy V_s of unit charges along the line segment OP corresponding to the quasi-harmonic model with $\delta = 2$ Å, 1 Å, and 0.5 Å, respectively.

C. Convergence of the proposed numerical method as $L \to \infty$

To investigate the convergence of the proposed numerical method in terms of L, the number of sublayers to discretize the transition layer in a three-layer dielectric model, here we consider its application to the linear and the cosine-like dielectric models with $\delta = 2$ Å.

We calculate the self-polarization energies of 1000 unit charges equally spaced along the line segment OP, and the numerical results are compared to those obtained by the proposed numerical method using $L = 3,000$ to calculate the L_2-relative errors in the self-polarization energy, which are displayed in Fig. 7. More precisely, the L_2-relative error E in the self-polarization energy is defined as

$$E = \sqrt{\frac{\sum\limits_{1\le i\le 1000}\left(V_s^{(L)}(\mathbf{r}_i) - V_s^{(3000)}(\mathbf{r}_i)\right)^2}{\sum\limits_{1\le i\le 1000}\left(V_s^{(3000)}(\mathbf{r}_i)\right)^2}}, \tag{72}$$

where $V_s^{(L)}(\mathbf{r}_i)$ denotes the computed self-polarization energy of a unit charge at $\mathbf{r}_i$ by using the numerical method with L sublayers. As can be seen, the results clearly demonstrate the convergence of the proposed numerical method as $L \to \infty$. Based on this, it is reasonable to believe that, for general three-layer dielectric models, the proposed numerical method should be able to recover the exact solution of the corresponding Poisson equation as $L \to \infty$.

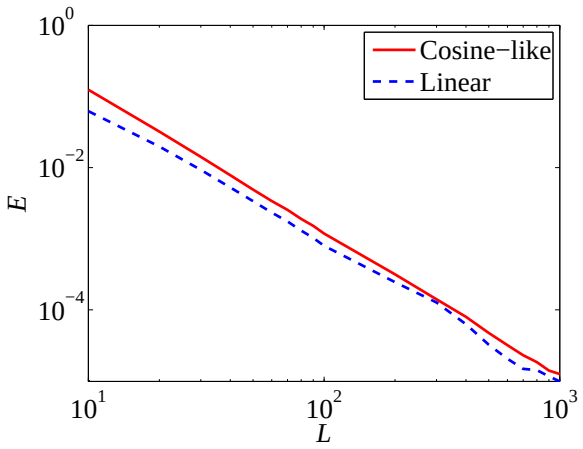

FIG. 7: (Color online) L_2-relative error E in the self-polarization energy corresponding to the linear and the cosine-like models with $\delta = 2$ Å, respectively, using the proposed numerical method with various L values.

Next, in Fig. 8 we show the self-polarization energy for the QD corresponding to the foregoing three three-layer dielectric models with $\delta = 2$ Å, respectively. It is evident that the choice of different dielectric permittivity profiles for the dielectric transition layer modifies both the strength and the functional form of the potentials, although all three forms of $\varepsilon(\xi)$ can eliminate the mathematical divergence present when $\delta = 0$. However, since the

derivative of $\varepsilon(\xi)$ in both the quasi-harmonic and the linear models is discontinuous at the both boundaries of the transition layer, the self-polarization energy corresponding to these two models exhibits differential singularity at these locations as well.

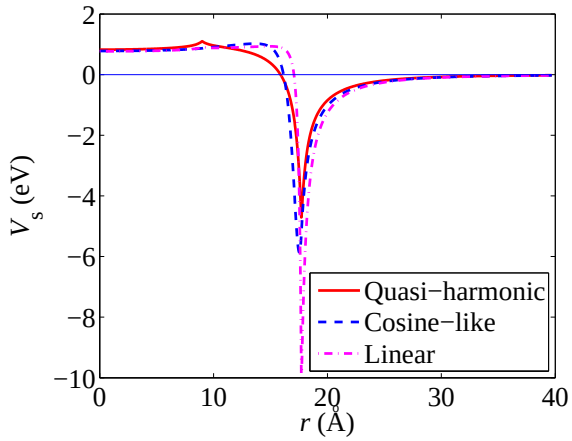

FIG. 8: (Color online) Self-polarization energy V_s as a function of r for several three-layer dielectric models with $\delta = 2$ Å. Solid line, the quasi-harmonic model with using the analytical solution; dashed and dot-dashed lines, the cosine-like and the linear models with using the proposed numerical method.

D. The dielectric ellipsoid approaches a sphere.

Finally, let us examine the case when the dielectric ellipsoid approaches a sphere for the sake of further validation of the results obtained in the present paper. While it may be possible to theoretically prove that (58) will reduce to Eq. (11) of Ref. [11] and (71) to Eq. (46) of Ref. [11], we shall compare these equations numerically in order to avoid long, tedious mathematics. To this end, we consider a spherical QD given by $x^2 + y^2 + z^2 = 10^2$ but still assume $\varepsilon_i = 12.6$ and $\varepsilon_o = 1$. We calculate the self-polarization energies of 200 unit charges (in atomic unit) uniformly distributed along the line segment with two endpoints $(0, 0, 0)$ and $(0, 0, 20)$ corresponding to the quasi-harmonic and the cosine-like three-layer dielectric models, respectively. The results are displayed in Fig. 9. In all of these simulations, the width of the transition layer is fixed with $\delta = 5$ Å, and when the numerical methods are involved, the number of sublayers used to discretize the transition layer is set to $L = 1000$. However, the imposed upper limit of n is set to $N = 4000$ when the QD is

regarded as a sphere and $N = 62$ as an ellipsoid, respectively. Also, it should be pointed out that, when treating the spherical QD as a limiting case of an ellipsoid, we actually use $x^2/10.01^2 + y^2/10^2 + z^2/9.99^2 = 1$ so that the two semi-focal distances k and h do not become zero; otherwise the formulae obtained for the ellipsoidal geometry cannot be used directly. As can be seen, the numerical results obtained by treating the spherical QD as a limiting case of an ellipsoid, and thus applying the formulae presented in the present paper, are in excellent agreement with those obtained by directly using the formulae developed in Ref. [11] for the spherical geometry, suggesting once again the correctness of the analytical solution for the quasi-harmonic three-layer model as well as the robustness of the numerical method for general three-layer models presented in this paper for the ellipsoidal geometry.

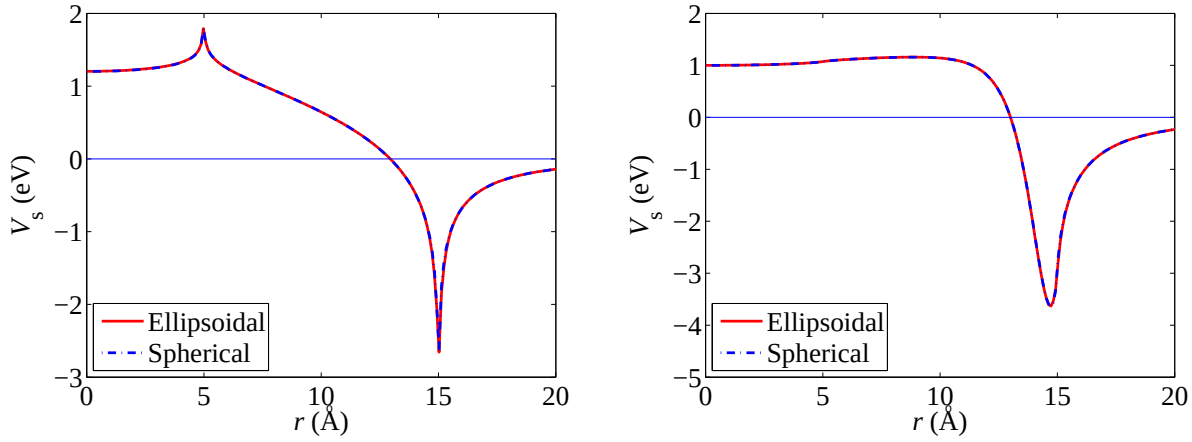

FIG. 9: (Color online) Self-polarization energy V_s of unit charges along the line segment with two endpoints $(0, 0, 0)$ and $(0, 0, 20)$ when a spherical QD given by $x^2 + y^2 + z^2 = 10^2$ is considered. The dash-dotted lines are the results calculated by directly using the analytical solution of the quasi-harmonic three-layer model and the robust numerical method for general three-layer models in the spherical geometry developed in Ref. [11], while the solid lines are the results obtained by treating the spherical QD as a limiting case of an ellipsoid, and thus applying the formulae presented in the present paper. In the latter case, a small perturbed spherical QD given by $x^2/10.01^2 + y^2/10^2 + z^2/9.99^2 = 1$ is actually used in order that the two semi-focal distances k and h of the resulting ellipsoid do not become zero. $\delta = 5$ Å. (a) Analytical solutions for the quasi-harmonic three-layer models in the spherical and the ellipsoidal geometries; (b) Numerical solutions for the cosine-like three-layer models in these two geometries.

VII. CONCLUDING REMARKS

The novel quasi-harmonic three-layer dielectric model for calculating generalized Coulomb and self-polarization potentials in heterogeneous dielectric media has been extended to the ellipsoidal geometry. The explicit analytical series solutions for the corresponding Poisson equation in terms of the ellipsoidal harmonics have been developed. The quasi-harmonic dielectric model can overcome the inherent mathematical divergence in the self-polarization energy that exists in the simple step-like dielectric model. Furthermore, a robust numerical procedure working for general three-layer dielectric models has been presented. The key component of this numerical method is to subdivide the transition layer of the underlying three-layer model into multiple sublayers, and then in each one of them approximate the select dielectric function of the transition layer by one of the quasi-harmonic functional form. The results presented in this paper can find their applications in many areas that involve the calculation of the generalized Coulomb potential such as simulations of ellipsoidal semiconductor quantum dots, molecular dynamics simulations of elongated, non-spherical or non-spheroidal bio-macromolecules, etc.

Acknowledgments

The authors thank the support of the National Natural Science Foundation of China (Grant No. 10971181) for the work reported in this paper.

References

[1] C. Xue and S. Deng, Commun. Comput. Phys. **8**, 374 (2010).

[2] L. E. Brus, J. Chem. Phys. **80**, 4403 (1984).

[3] M. Lannoo, C. Delerue, and G. Allan, Phys. Rev. Lett. **74**, 3415 (1995).

[4] P. G. Bolcatto and C. R. Proetto, J. Phys. Condens. Matter **13**, 319 (2001).

[5] A. Okur and C. Simmerling, in *Annu. Rep. Comput. Chem.*, edited by D. C. Spellmeyer (Elsevier, Amsterdam, 2006), vol. 2, chap. 6, pp. 97–109.

[6] J. G. Kirkwood, J. Chem. Phys. **2**, 351 (1934).

[7] S. Deng, J. Electrostatics **66**, 549 (2008).

[8] S. Deng, J. Electrostatics **67**, 807 (2009).

[9] D. V. Redzic and S. S. Redzic, J. Phys. D: Appl. Phys. **38**, 3991 (2005).

[10] P. Qin, Z. Xu, W. Cai, and D. Jacobs, Commun. Comput. Phys. **6**, 955 (2009).

[11] S. Deng, Comput. Phys. Commun. **181**, 787 (2010).

[12] P. G. Bolcatto and C. R. Proetto, Phys. Stat. Sol. **220**, 191 (2000).

[13] J. L. Movilla and J. Planelles, Comput. Phys. Commun. **170**, 144 (2005).

[14] C. Xue and S. Deng, Phys. Rev. E **81**, 016701 (2010).

[15] P. M. Morse and H. Feshbach, *Methods of Theoretical Physcs* (McGraw-Hill, New York, 1953).

[16] T. Miloh, Israel J. Tech. **11**, 63 (1973).

[17] J. W. Perram and P. J. Stiles, Proc. R. Soc. Lond. A **349**, 125 (1976).

[18] T. Miloh, J. Ship Research **23**, 66 (1979).

[19] J. C. E. Sten, J. Electrostatics **64**, 647 (2006).

[20] L. C. Lew Yan Voon and M. Willatzen, J. Phys. Condens. Matter **16**, 1087 (2004).

[21] L. Serra, A. Puente, and E. Lipparini, Phys. Rev. B **60**, R13966 (1999).

[22] K. Hirose and N. S. Wingreen, Phys. Rev. B **59**, 4604 (1999).

[23] G. Cantele, D. Ninno, and G. Iadonisi, J. Phys. Condens. Matter **12**, 9019 (2000).

[24] K. G. Dvoyan, E. M. Kazaryan, and L. S. Petrosyan, Physica E **28**, 333 (2005).

[25] E. W. Hobson, *The Theory of Spherical And Ellipsoidal Harmonics* (Cambridge University Press, Cambridge, England, 1931).

[26] R. Garmier and J.-P. Barriot, Celestial Mech. Dyn. Astr. **79**, 235 (2000).

[27] A. Irimia, J. Phys. A: Math. Gen. **38**, 8123 (2005).

[28] S. Ritter, ZAMM·Z. Angew. Math. Mech. **78**, 66 (1998).

[29] H.-J. Dobner and S. Ritter, Computing **60**, 81 (1998).

[30] G. Dassios and F. Kariotou, J. Math. Phys. **44**, 220 (2003).

[31] G. Dassios and T. Miloh, **57**, 757 (1999).

[32] D. L. Clements, Comput. Mech. **22**, 26 (1998).

[33] A. Sihvola and I. V. Lindell, J. Electro. Waves Appl. **3**, 37 (1989).

[34] I. V. Lindell, M. E. Ermutlu, and A. H. Sihvola, IEE Proc.-H **139**, 186 (1992).

[35] A. Sihvola and I. V. Lindell, J. Electro. Waves Appl. **2**, 741 (1988).

[36] J. L. Movilla and J. Planelles, Phys. Rev. B **71**, 075319 (2005).